Supporting Information

Kim et al. 10.1073/pnas.1113890109

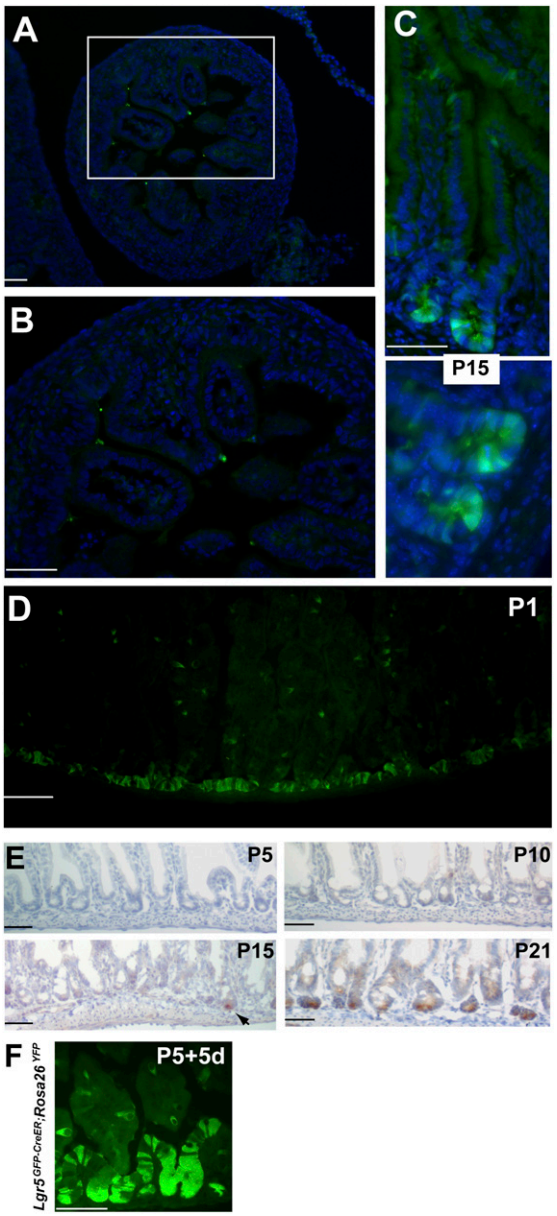

Fig. S1. Location of Lgr5^{+} cells during mouse development. (*A* and *B*) No GFP staining is detected at embryonic day 15 (E15) in *Lgr5*$^{GFP\text{-}CreER}$ mouse embryonic duodenum. The boxed area in *A* is magnified in *B*. (*C*) Example of GFP expression at postnatal day 15 (P15) in *Lgr5*$^{GFP\text{-}CreER}$ duodenum, showing some GFP^{-} cells in the space between GFP^{+} cells (*C*) compared with earlier stages (see Fig. 1 *B* and *C*). (*D*) Distribution of Lgr5 (GFP^{+}) cells in intestinal intervillus spaces 1 d after birth (P1). (*E*) Lysozyme immunohistochemistry in mouse small intestines between postnatal day 5 (P5) and postnatal day 21 (P21). Paneth cells start to express lysozyme around P15. (*F*) YFP expression in intestinal villi in *Lgr5*$^{GFP\text{-}CreER}$; *Rosa26*^{YFP} mice 5 d after a single tamoxifen injection administered at P5. (Scale bars: 50 μm.)

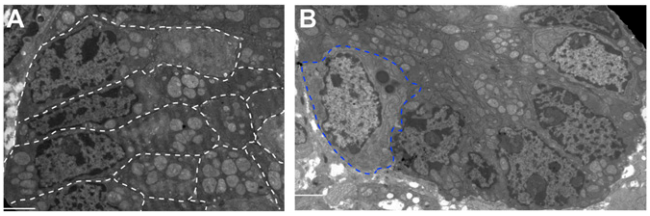

Fig. S2. Electron micrographs of sample postnatal day 10 (P10) intervillus regions. (*A*) Cells with crypt base columnar cell (CBC)-like ultrastructure (demarcated by dashed white lines) cluster at the bottom of intervillus regions, without intervening cells. (*B*) Rare immature Paneth cells (demarcated here by the dashed blue line) appear in one of ~10 intervillus regions, which contain mostly CBCs. (Scale bars: 2 μm.)

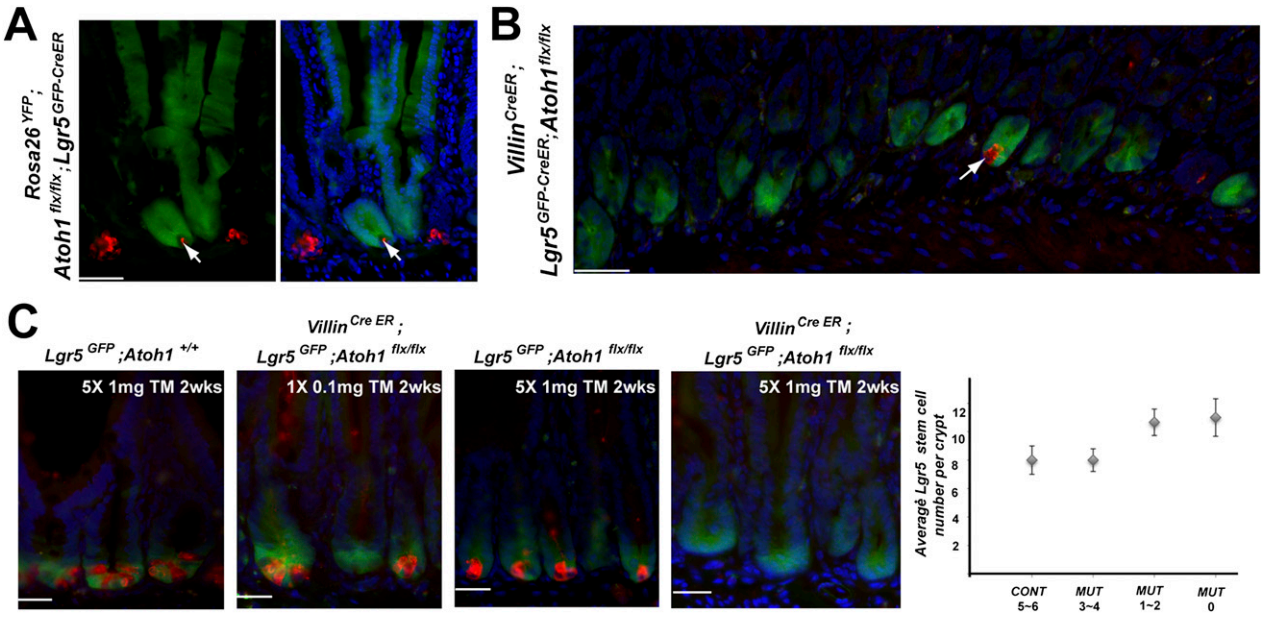

Fig. S3. Lgr5^{+} (GFP^{+}) stem-cell quantification in crypts depleted of Paneth cells. (*A*) (*Left*) Lineage tracing through the *Rosa26*^{YFP} reporter shows that residual YFP^{-} Paneth cells (arrow) originated in a previous renewal cycle, before Cre-mediated recombination. (*Right*) DAPI nuclear stain added to image in left panel. (*B*) Very rare Paneth cells (arrow, fewer than 1 per 500 crypts) were detected in *Villin*^{CreER};*Lgr5*$^{GFP\text{-}CreER}$;*Atoh1*$^{flx/flx}$ mice, likely reflecting escape from Cre recombination. (*C*) Lgr5^{+} (GFP^{+}) stem cells are not decreased when Paneth cell number is reduced and are slightly increased in the total absence of Paneth cells. Fluorescence micrographs show sample crypts from control (far left panel) and mutant mice with Paneth cell numbers reduced to three or four per crypt (second panel from left), one or two per crypt (third panel from left), or none (far right panel). Mouse genotypes are indicated, and the graph quantifies Lgr5^{+} CBCs in crypts containing three or four Paneth cells, one or two Paneth cells, or none. At least four mice and 50 crypts per mouse were analyzed for each class. Error bars represent SD. (Scale bars: 50 μm.)

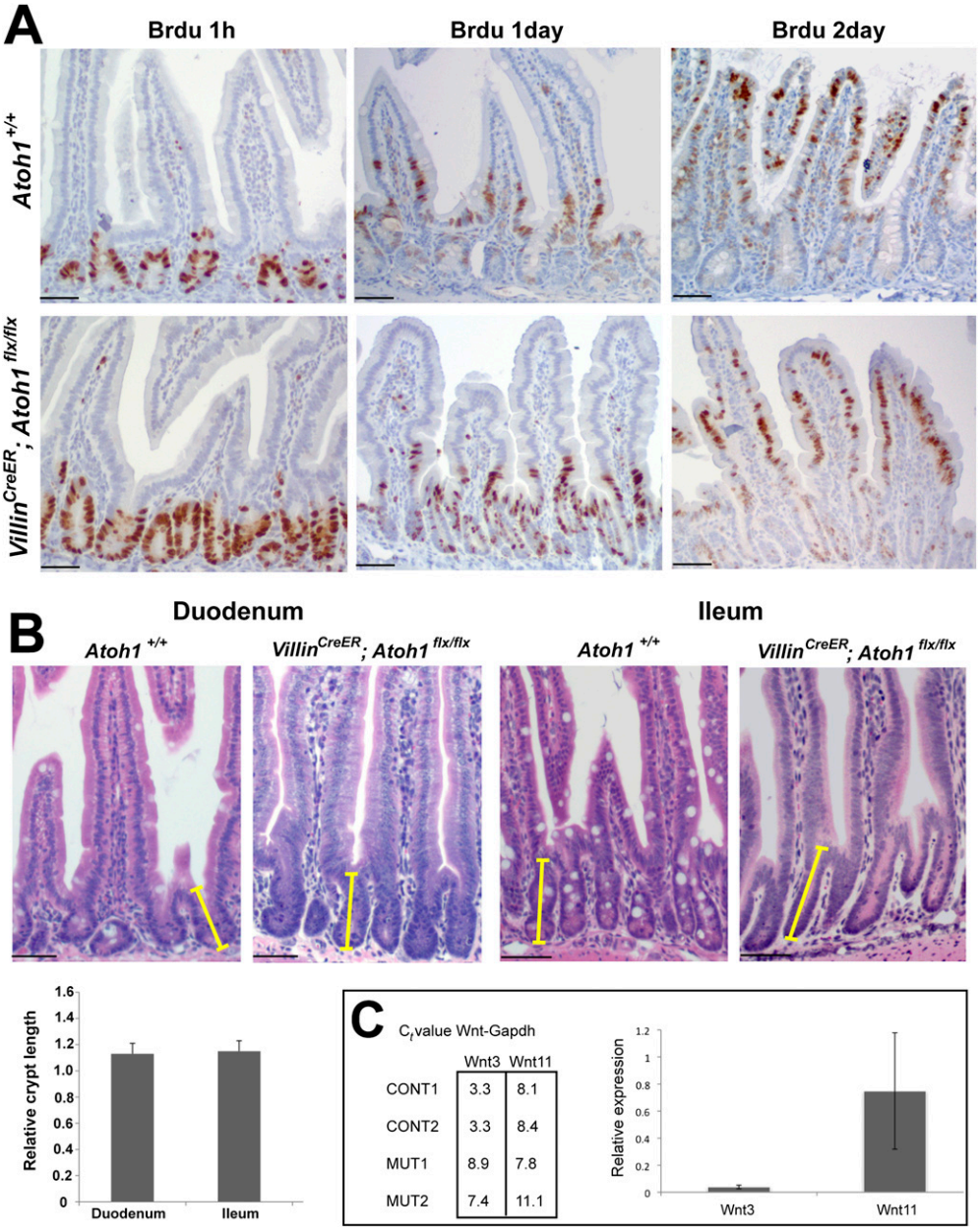

Fig. S4. Turnover rate of intestinal epithelium, crypt height, and Lgr5^{+} cell expression of Wnts in the absence of Paneth cells. (*A*) BrdU tracing shows that epithelial cells in Paneth cell-depleted crypts turn over at rates similar to wild-type cells. *Atoh1*$^{+/+}$ and *Villin*^{CreER};*Atoh1*$^{flx/flx}$ mice were injected with BrdU (50 mg/kg), and BrdU-labeled intestinal cells were followed for 1 h, 1 d, and 2 d. (*B*) Paneth cell-depleted crypts are 13–15% taller than controls. H&E staining of *Atoh1*$^{+/+}$ and *Villin*^{CreER};*Atoh1*$^{flx/flx}$ duodenum and ileum. At least 100 crypts were measured in each of three intestines from each group of mice. (*C*) No expression of *Wnt11* and decreased *Wnt3* expression in Lgr5^{+} stem cells sorted by flow cytometry from Paneth cell-depleted crypts. Changes in threshold cycle (ΔC_t) values from quantitative RT-PCR analysis were calculated relative to *Gapdh* mRNA, and expression in cells derived from mutant mice (MUT1 and MUT2) is graphed relative to wild-type Lgr5^{+} cells (CONT1 and CONT2). Error bars represent SD. (Scale bars: 50 μm.)